GALACSI integration and functional tests

P.La Penna*, S.Ströbele, E.Aller Carpentier, J.Argomedo, R.Arsenault, R.D.Conzelmann, B.Delabre, R.Donaldson, M.Duchateau, E.Fedrigo, F.Gago, N.Hubin, J.Quentin, P.Jolley, M.Kiekebusch, J.P.Kirchbauer, B.Klein, J.Kolb, H.Kuntschner, M.Le Louarn, J.L.Lizon, P.-Y.Madec, A.Manescau, L. Mehrgan, B. Sedghi, M.Suárez Valles, C.Soenke, S.Tordo, J.Vernet, S. Zampieri [a]

[a] European Southern Observatory; Karl-Schwarzschild-Strasse 2; D-85748 Garching; Germany

ABSTRACT

GALACSI is the Adaptive Optics (AO) module of the ESO Adaptive Optics Facility (AOF) that will correct the wavefront delivered to the MUSE Integral Field Spectrograph. It will sense with four 40×40 subapertures Shack-Hartmann wavefront sensors the AOF 4 Laser Guide Stars (LGS), acting on the 1170 voice-coils actuators of the Deformable Secondary Mirror (DSM).
GALACSI has two operating modes: in Wide Field Mode (WFM), with the four LGS at 64" off axis, the collected energy in a 0.2"×0.2" pixel will be enhanced by a factor 2 at 750 nm over a Field of View (FoV) of 1'×1' using the Ground Layer AO (GLAO) technique. The other mode, the Narrow Field Mode (NFM), provides an enhanced wavefront correction (Strehl Ratio (SR) of 5% (goal 10%) at 650 nm) but in a smaller FoV (7.5"×7.5"), using Laser Tomography AO (LTAO), with the 4 LGS located closer, at 10" off axis.
Before being shipped to Paranal, GALACSI will be first integrated and fully tested in stand-alone, and then moved to a dedicated AOF facility to be tested with the DSM in Europe. At present the module is fully assembled, its main functionalities have been implemented and verified, and AO system tests with the DSM are starting. We present here the main system features and the results of the internal functional tests of GALACSI.

Keywords: Adaptive Optics, AOF, GLAO, LTAO, MUSE, Sodium Laser Guide Star, Deformable Secondary Mirror.

1. INTRODUCTION

GALACSI is developed in the frame of the Adaptive Optics Facility AOF [1]. It will be mounted on the Nasmyth platform B of VLT UT4, to provide to MUSE an AO corrected wavefront in the MUSE [2] wavelength observation range (between 465 and 930 nm). GALACSI has 2 operational modes: in WFM it provides a seeing enhancement by means of ground layer correction; in NFM it provides modest SR at visible wavelengths. The main requirements and expected performances of GALACSI are described in [3]. In short, in WFM the goal requirement is to increase the ensquared energy within a MUSE spatial pixel of 0.2"×0.2" by a factor 2 at 750nm and for seeing conditions from 0.6" to 1.1", using one tip tilt reference star of magnitude 17.5 or brighter located outside the scientific FoV of MUSE . Sky coverage larger than 80% at the galactic pole is achieved thanks to four LGS, also located outside the MUSE field of view, at 64". AO correction works therefore in the GLAO correction [4] scheme. In NFM [4] the requirement is to provide SR >5% at 650 nm for 0.6" seeing with a Near Infrared (NIR) Tip-Tilt (TT) source of magnitude 15 in J-H band. Four LGS at 10" off axis are used, outside the NFM FoV of MUSE (a square of 7.5" side). With close LGS the whole turbulence around the telescope axis is probed, and the best wavefront error estimate and correction is performed through LTAO) [4] algorithms. To attain the required SR, the Tip-Tilt Star (TTS) has to be close to the telescope axis, that is in the MUSE FoV. In order not to reduce the throughput to MUSE, a dedicated TT sensor (IRLOS, InfraRed Low Order Sensor), that gets only NIR light separated by a dichroic after the MUSE derotator, is attached for this purpose below the MUSE Fore Optics.
Besides the DSM [5], important components like the Wavefront Sensors (WFS) and the Real-time computer (RTC) are shared with other AOF systems. The WFS are based on the ESO AO camera [6] with an E2V CCD-220 with 240×240 pixels with a pixel size of 24μm. It facilitates an electron multiplication readout register and full frame rate of 1000 Hz with a read noise below $1e^-$ rms. The tip tilt sensor will use the ESO deep depletion AO camera [7] without lenslet array, while for the 4 LGS WFSs a lenslet array of about 4.4mm focal length, with 40×40 sub-apertures is placed in front of the CCD. The pixel scale of an individual sub-aperture of the WFS is 0.83"/pixel giving a maximum FoV per sub-aperture of almost 5"×5". The RTC will be a dedicated unit based on the SPARTA platform [8] performing the AO camera data handling, centroids estimation and DM command calculation with a latency of less than 200μs at the

default AO loop rate of 1000Hz. The reconstruction is based on a Vector Matrix Multiplication. SPARTA includes also a numerical processing cluster allowing the storage of large datasets of real time data and offline data processing.

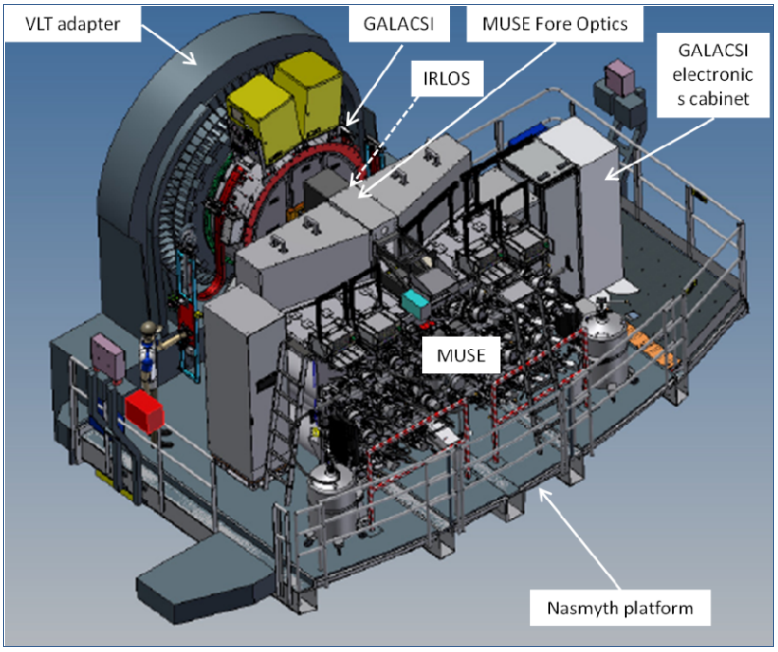

Figure 1: 3D mechanical model of GALACSI with MUSE on the Nasmyth platform B of UT4. The two upper electronics cabinets are visible between the rotator and MUSE. IRLOS, not visible in the figure, is located under the MUSE Fore Optics

2. GALACSI LAYOUT

GALACSI is an over 3-m-high and 1-ton-heavy complex AO module, including internal calibration and commissioning units, truth sensors, tracking and closed loop functionalities. All the opto-mechanical components are enclosed inside a cylindrical structure attached to the VLT adapter and located on the VLT focal plane, between the telescope and MUSE, with exception of the NFM TT sensor IRLOS, which is attached at the end of the MUSE fore optics extension beam.

To maintain a constant registration between the patterns of the WFS sub-apertures and the actuators on the DSM the GALACSI main assembly co-rotates to the telescope pupil, when the telescope altitude changes. The field as view by GALACSI turns therefore according to the parallactic angle. For proximity reasons, two electronics cabinets (WFS power supplies and piezo controller) are mounted on the upper part of the cylindrical structure, and three other cabinets containing actuator and control electronics are attached to the lower part of it. Two lateral columns fixed on the platform support the connectors for the electrical cables wrap, data transmitting and network fibers, cooling pipes (Figure 2). The opto-mechanics and control electronics are arranged on the Nasmyth platform of the VLT UT4 (Figure 1). The SPARTA electronics is ranged in a dedicated cabinet located in a space below the telescope platform.

The detailed specifications and goal performances driving the opto-mechanical design of GALACSI are described in [3]. The overall optical layout of the system is shown in Figure 3.

In WFM the 1'×1' MUSE field passes unperturbed through the hole of an annular mirror, whereas an annular field of 3.6' outer diameter containing the TTS and the LGS is reflected by the annular mirror to the GALACSI TT and LGS sensors. In NFM a dichroic mirror (NFM dichroic) with reflective narrowband at 589nm reflects the LGS to the GALACSI LGS sensors, letting all the other wavelength pass through. The VLT Nasmyth focus is located at the center of the hole of this annular mirror. Lids or shutters, to close the openings of the GALACSI main assembly when it is not used, are also provided, in order to minimize dust contamination.

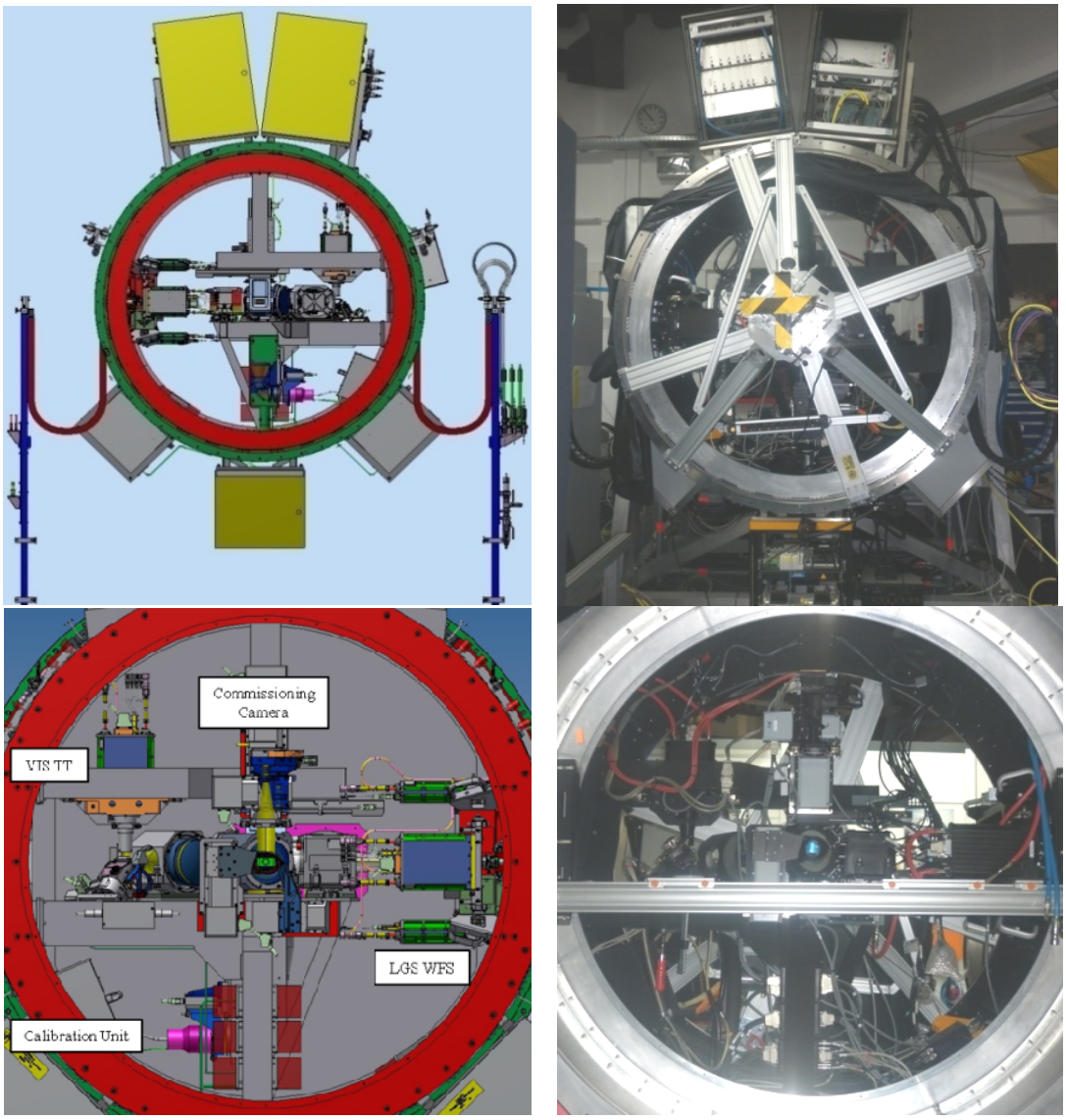

Figure 2: Top left: mechanical model of GALACSI, as view from the VLT side. Top right: GALACSI during the integration and testing phase in ESO integration hall at Garching (the cross bars in front of it are supporting the alignment tools). Bottom left: mechanical model of GALACSI, as view from the MUSE side. Bottom right: picture of the assembled instrument (the horizontal bar is for integration purposes), from the same point of view.

One TT Sensor (an ESO Deep Depletion AO camera without lenslet array) provides WFM TT correction. On the TTS path a large collimator forms a pupil on a beam steering mirror (Field Selector, FS). This allows to precisely direct part of the TT FoV to the TTS camera. The pixel scale is 0.167" leading to a maximum FoV of 40". In closed loop operation only a small window with 3"×3" around the TTS will be used.
Four high order Shack Hartman (SH) sensors based on the ESO AO Cameras [6] detect the four LGS. On the LGS path a Focus Compensator (FCO) corrects the LGS focus variation and produces a collimated beam with an intermediate pupil. The reimaging lens forms an image plane where a reflective pyramid sends the beams of the 4 LGSs to the corresponding optical trains (only one of them is shown in Figure 3). Two sets of relay lenses form first an intermediate pupil image on a piezo tip-tilt steerable mirror, used to stabilize the LGS image, and then another pupil on the micro lens array of the SH WFS camera. The four LGS are at 64" in WFM. To switch to the NFM configuration the LGS are pointed closer on to the other (using the steering capability of the LGS launching telescopes [9]) to 10" off axis e.g. their respective beams fall onto the central hole of the annular mirror, where the NFM dichroic mirror is inserted by a translation stage. The NFM dichroic mirror reflects the LGS light towards the LGS optical path as in WFM and transmits the light in the wavelength range from 465nm to 1800nm. The position of the LGS outside of the

scientific FoV helps in reducing the sky contamination by LGS scattered light. To further damp the scattered LGS light it is foreseen to place a notch filter in the MUSE fore optics.

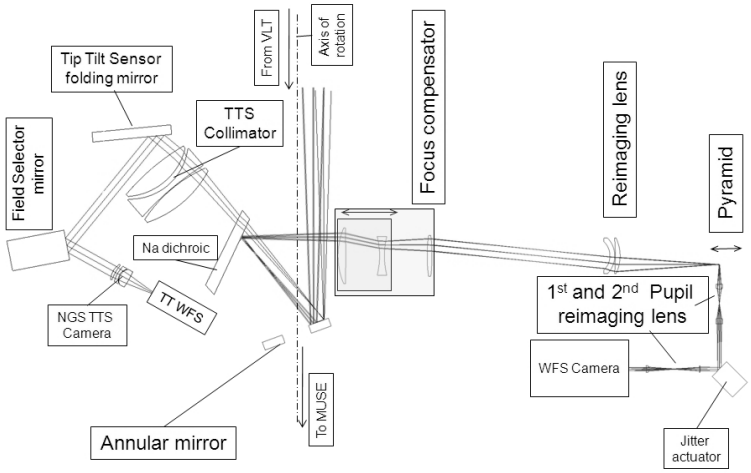

Figure 3: Optical scheme of GALACSI in WFM configuration (the Calibration Unit is not in the figure, and only one LGS-WFS is shown).

A Commissioning Camera with sufficient field coverage and pixel size allows performance measurements. The camera is placed at the side of GALACSI where the beam exits the assembly (in Figure 3 only the WFM configuration is shown).

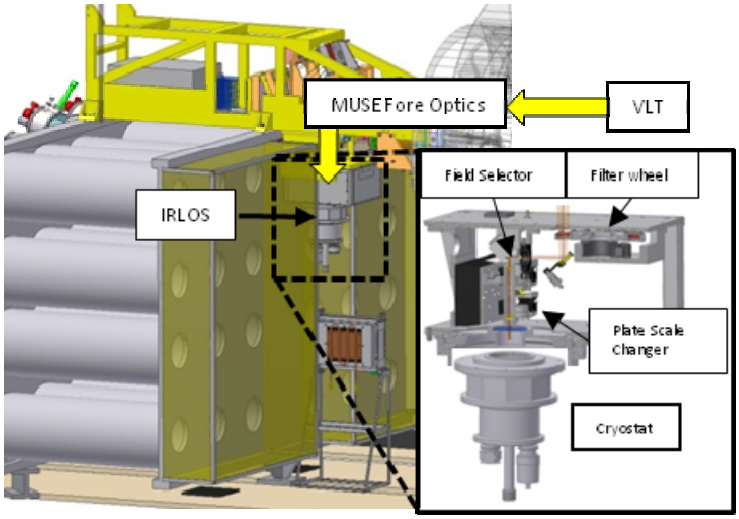

Figure 4: location of the IRLOS truth sensor for GALACSI NFM: IRLOS is placed inside MUSE, below the MUSE Fore Optics, after GALACSI and the MUSE optical derotator.

This avoids obscuration and allows to use and test GALACSI the same way as during normal operations. The light is picked up and sent to the Commissioning Camera by a thin (1-mm-thick) 50% Beam Splitter (BS) placed after the VLT focus, that is on the light train going to MUSE. The BS is inserted in the light beam by a translator. Owing to the small thickness of the BS, the beam shift to MUSE is minimal, this allowing, during commissioning or checks, to use the Commissioning Camera while MUSE is also measuring. During scientific acquisition the BS is taken out from the light beam. The system includes a focusing stage.

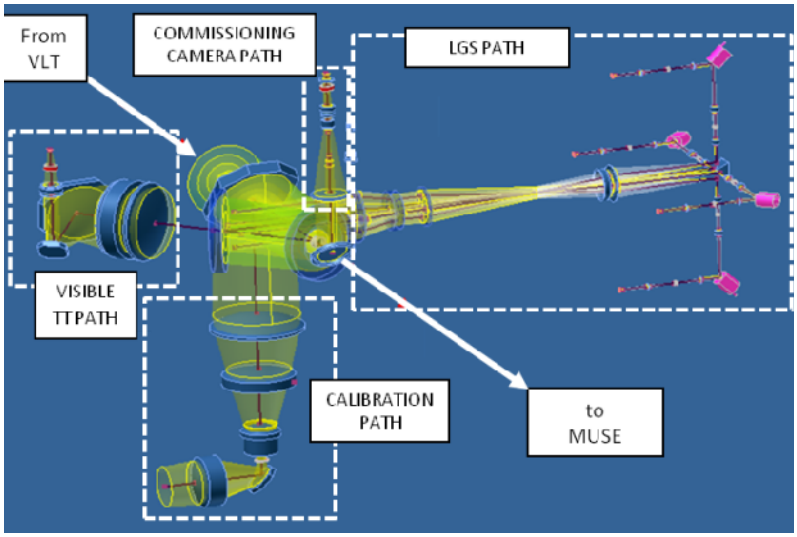

Figure 5: 3D opto-mechanical model of GALACSI in WFM, showing the different systems of the module. The Calibration Unit provides the light sources for all the other internal systems (Visible TT, LGS and IRLOS, not shown in the figure). The Calibration Camera is used for image check.

For TT and focus sensing the NIR light in the wavelength range from 950nm to 1800nm is separated by a dichroic mirror and sent to the 2×2 sub-aperture SH sensor IRLOS, attached to the fore optics assembly of MUSE (Figure 4, left).
For the calibration of the FS and the measurement of the reference slopes of the WFS several point sources are needed to simulate NGSs and LGS. A Calibration Unit (CU) simulating point sources is moveable in the field and focus (Figure 4, right). The light of the Calibration sources can be fed into the system by inserting the CU folding mirror into the entrance beam path. All the tests performed so far have been made using the CU sources.

3. GALACSI INTEGRATION AND TESTING IN EUROPE

Before being shipped to Paranal GALACSI has to be integrated and tested first in stand-alone and then in closed loop with the DSM on the ASSIST test facility [10]. The module is at present almost fully integrated and most of the internal functional tests have been performed. Using the CU as light source, the TT, LGS and Commissioning Path have been tested separately.

3.1 Calibration Unit

In Figure 6 are shown the optical design, the opto-mechanical model and the actual implemented CU. Since the focal plane is embedded between optical components, there is no space to place e.g. fiber point sources directly in the focus, hence a reimaging objective is required .The CU optics is a telecentric system, reproducing a light beam with the same *f*/# (=15.2) and same focus position of VLT at the Nasmyth focus inside GALACSI with an internal pupil stop corresponding to the VLT one. All the sources (NGS and LGS) are emitted by fibers arranged on the same input fiber plate. The distribution of the sources on the fiber plate is shown in Figure 7.

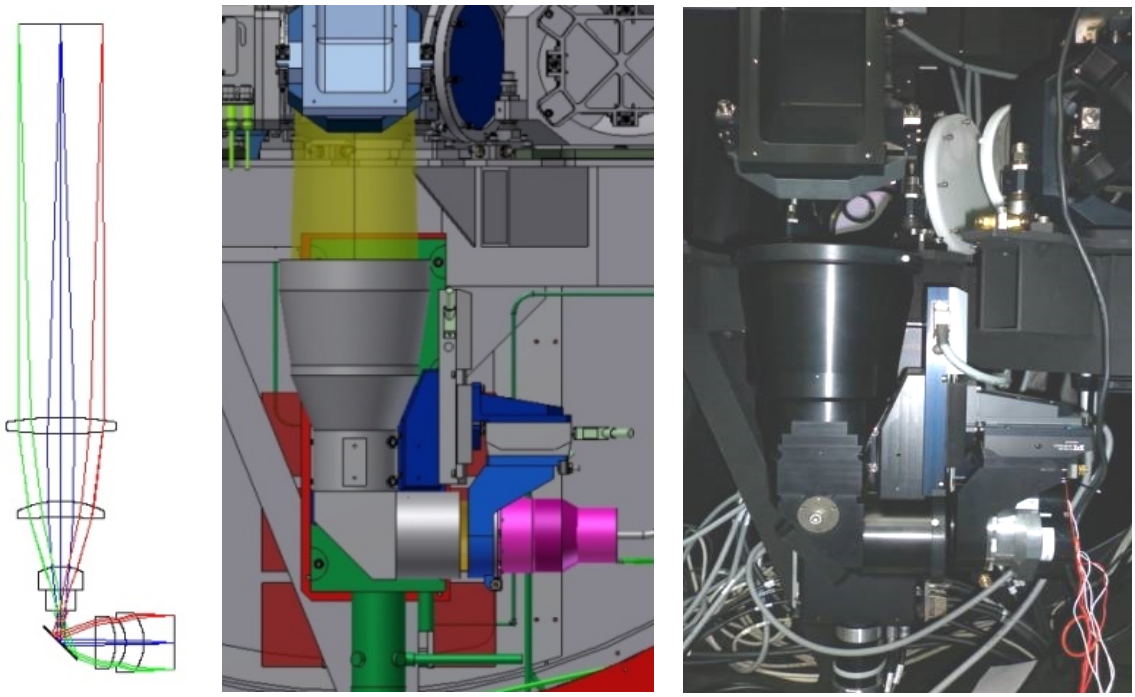

Figure 6: From left to right: optical scheme of the Calibration Unit. Mechanical model. Picture of the integrated system (at a different focal position with respect to the central drawing.

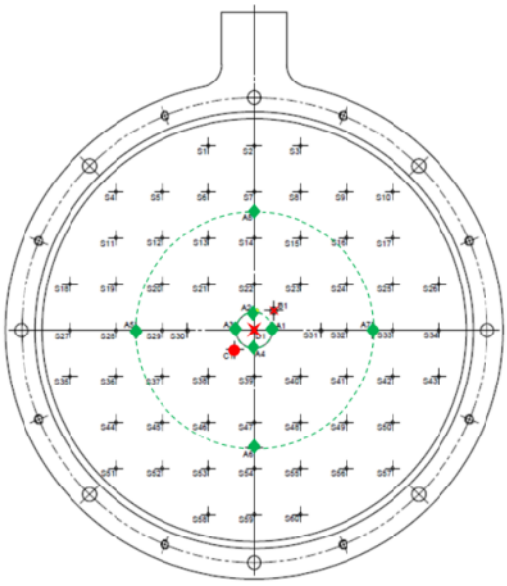

Figure 7: Distribution of the sources on the CU fiber plate: a grid of 60 visible sources (fiber core≅100 μm) for TT and FS testing, two rings of LGS sources (WFM and NFM, fiber core ≅ 500 μm) for LGS testing, one extended visible-IR source close to the center (fiber core≅600 μm) for IRLOS, one small visible-IR source in the middle (fiber core ≅9 μm) and one sub-diffraction limited source close to the center for general purpose. All fibers have NA>0.2, transmitting light produced by halogen lamps (visible and IR) and leds (589 nm).

The focus position change from NGS to LGS (of the order of 150 mm for a 100 km far LGS) is performed by shifting the whole unit along the VLT axis with a translator by the amount corresponding to the difference in focus position between the two kinds of guiding stars. The translation stage allows to scan a guiding star position from infinite to about 100 km on-sky equivalent height.

3.2 Tip-Tilt path

As described above and in [3], the tip tilt stars in GALACSI WFM is off-axis, located outside the 1' MUSE field and within an annular surface. Since the field, as seen by GALACSI, rotates with the rate of the parallactic angle, the image of the TT star is kept in a stable position by a Field Selector (FS) mirror. The FS is a steering mirror located in a pupil. The circular trajectory of the TTS is approximated by the mechanical realization shown in Figure 8. The radial stage points to the radial distance between the field center and the TTS. A rotary stage points to the position angle and performs most of the tracking motion. Because of the beam incidence angle at the field selector of 45° the calculation of the actual position command of the FS stages requires a precise knowledge of the 3 dimensional orientation of the optical axis of the incoming beam, of the rotation axis of the FS turntable and the angle of the reflected beam. On top of the stringent requirements to the alignment one needs to precisely calibrate the zero positions of the FS radius and turn table stages. The sources are provided by the CU, covering the complete NGS field of GALACSI.

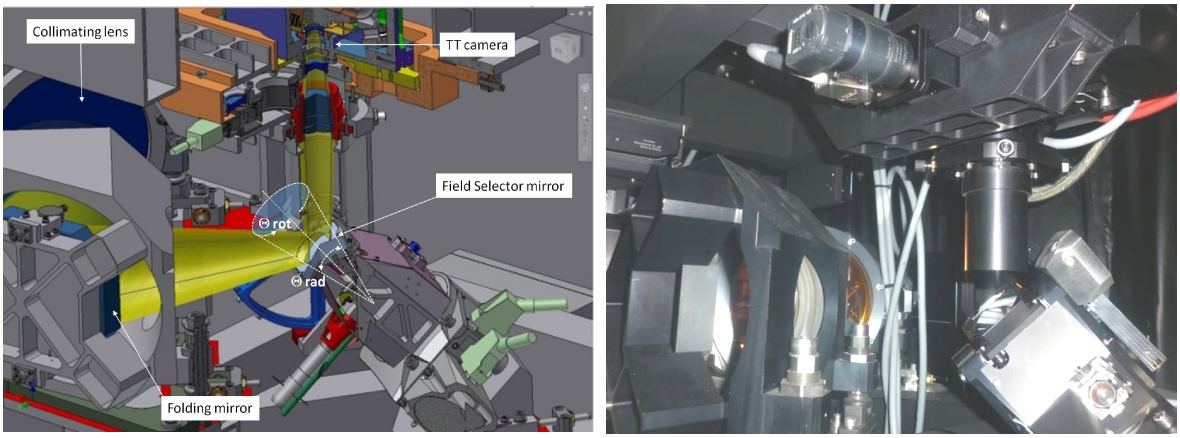

Figure 8: Left: optical scheme of the TT path: the FS mirror can rotate around a vertical axis (Θ rot) and tilt around a pivot (Θ rad). Right: photo of the FS+TT camera.

The verification that the FS and all components along the optical path up the TTS sensor was split in 3 parts. Each of them can be verified independently allowing for a systematic identification of error.

a. Static pointing verification
b. Tracking verification
c. Flexural testing

a. Static pointing verification

The FS was commanded to each of the sources and an image was recorded with the TT sensor camera. In an ideal world with perfect alignment and modeling of the field distortion of the TTS path optics the image of all sources would fall on the same pixel on the camera. However even after an extensive alignment and calibration of the system geometry the pointing error exceeded the specifications of 150 mas pp by roughly a factor 3.
The correction of the residual error was done by a pointing model where the corrections are described by 2D polynomials, one set of polynomials describes the error along the X axis, another one the Y axis. Finally the residual pointing error was 140mas pp (29 mas rms), which meets the specifications.

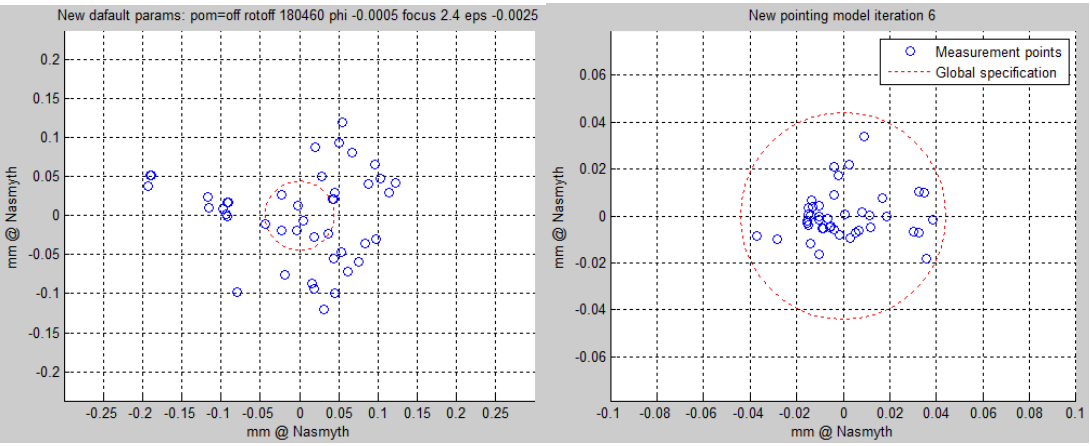

Figure 9: Pointing errors measured on 44 positions covering the TTS field of GALACSI. Left: after alignment and calibration of the geometry parameters. Right: with the implementation of the pointing model.

b. Tracking verification

The aim of the tracking verification is to verify the position control errors over the full range on both FS stages. Each stage needs to follow precisely, during an observation, a predefined trajectory at a very slow rate of few encoder tics per second. Due to the system inherent friction we expected some problems due to i.e. Stick –Slip. The motor control parameters of both stages had to be optimized to allow for a smooth motion. For the tracking test the assembly was following a simulated trajectory and at a rate of 50 samples per second the actual position and position error was recorded and the measurement analyzed. The tracking error of both stages is a the level of few mas rms, except for the times of the meridian crossing. Only during this short period, the following error of the stages becomes noticeable.

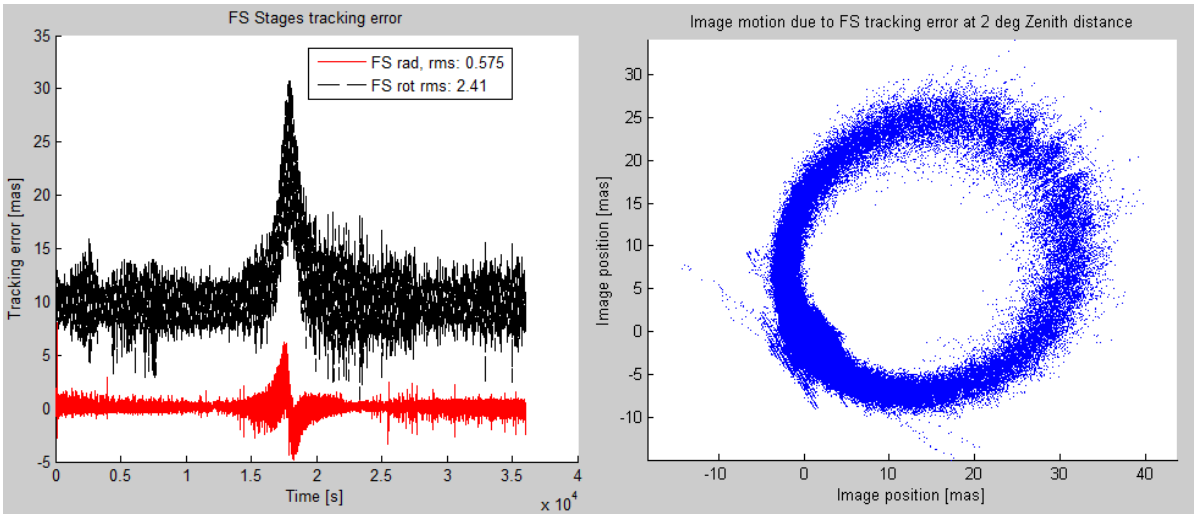

Figure 10: Left: time series of the following error of the FS-Radius and Rotation stages during a 10h tracking test with a meridian crossing 2 deg off Zenith. Right: simulated image wander during the simulated 10h observation

c. Flexure testing

Another origin of error in the TTS path could be caused by structural deformation due to the change of the gravity vector during an observation. This property was analyzed during the design phase of GALACSI by a detailed Finite Elements model. Because the model is usually based on a number of assumptions, it needs to be verified on the finally integrated system. For that purpose GALACSI will be installed on a telescope simulator which allows to rotate the whole System. On the Telescope side of GALACSI we will install a flexure test light source. This will generate an artificial Star on either the TTS or refocused to the LGS configuration be used on the LGS WFSs. The commissioning camera can be used in both configuration. GALACSI will be rotated to several positions covering the operational range

and at each position an image will be recorded. Analyzing the image drift versus rotator position will show the amplitude and evolution of the image drift with the angle. On the LGS path also the Pupil stability will be verified by measuring the flux centroid on the Shack Hartmann WFSs. At the time of writing the flexure tests are in preparation.

3.3 LGS path.

The LGS path system is shown in Figure 11. At the time of this paper one WFS has been fully aligned and tested, both in WFM and in NFM. The other three are being integrated. One detector is however sufficient to test all the main functionalities.
The alignment of the system is critical: pupil focusing on the steering mirror has to be better than 0.2mm; the pupil size has to be within ±0.25% with respect to the nominal diameter (5.76mm); the maximum pupil shift with respect to the lenslet array is 0.012mm, corresponding to 0.2% of the pupil; the perpendicularity on the lenslet array has not to exceed a quarter of a pixel (0.2" on sky). All these requirements have been met in the implemented system.

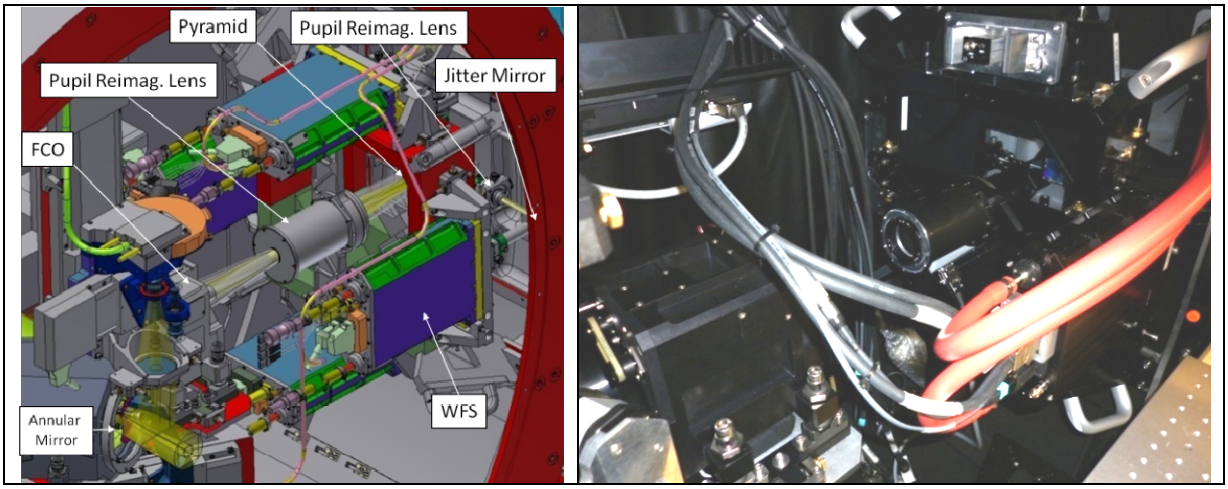

Figure 11: Left: Opto-mechanical model of the LGS path. Right: picture of the LGS path at present stage of integration: one LGS-WFS is integrated and aligned with its optics.

The expected pixel scale of 0.83"/pixel has also been verified using gaussian fit, both for WFM and NFM, at the level of 0.828"±0.015". The image produced after the alignment by the CU sources on the LGS WFS is shown in Figure 12. Of all the 1600 subapertures, 1240 are illuminated byt the light pupil. The SPARTA RTC acquires only these subapertures.
The optical LGS path is designed in order to yield a pupil of constant size and position on the WFS lenslet array, both in WFM and in NFM, and for the whole range of LGS distances. GALACSI is specified to operate for LGS distances between 80km to200 km, corresponding to a maximum altitude angle of 60° with respect to the the zenith and to a fluctuation of ± 10 km with respect to the expected average 90 km zenith Na layer centroid layer height [11]. The tracking of the Na distance is performed by moving the FCO, that builds up with the following relay optics a telecentric system able to position the pupil on the steering mirror and on the detector lenslet array, with the same final diameter The shift between WFM and NFM is obtained by offsetting the FCO and shifting by 14.5mm the separating pyramid (Figure 13).
The LGS-WFS pixels are acquired, and slopes are computed and processed, by the SPARTA RTC. After SPARTA wavefront Zernike decomposition, the lower order modes, tip, tilt and focus, are used to implement via SPARTA the LGS jitter control using the LGS steering mirror, and the LGS focus off-load using the FCO. The aim of the LGS jitter control is to keep the beam centered and aligned on the detector: LGS tip and tilts on the LGS-WFS are not produced by the atmospheric turbulence, and are rather to be ascribed to other effects, like internal alignment fluctuations, which have not to be corrected by the DSM. The LGS jitter mirror is mounted on a piezo actuator.

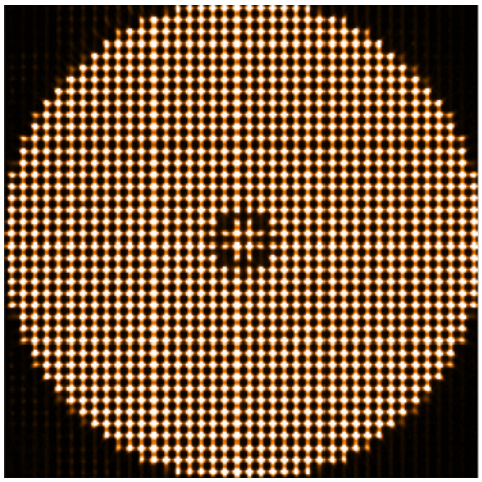

Figure 12: Image of the spots produced by the lenslet array on the LGS WFS using the CU LGS sources. The pupil diameter on the lenslet array is 5.76mm. The camera is a CCD-220 with 240×240 pixels with a pixel size of 24μm. The lenslet array includes 40×40 lenslets of about 4.4mm focal length. Of the total 1600 sub-apertures, only the 1240 illuminated ones are read by the RTC. A central mask is used for alignment purposes. The pixel scale of an individual sub-aperture of the WFS is 0.83"/pixel giving a maximum FoV per sub-aperture of almost 5"×5".

The tip and tilt measured by the LGS-WFS is used as an error signal to steer the mirror in closed loop and minimize the angle on the detector. The performances of the drift control loop are summarized in Figure 14.

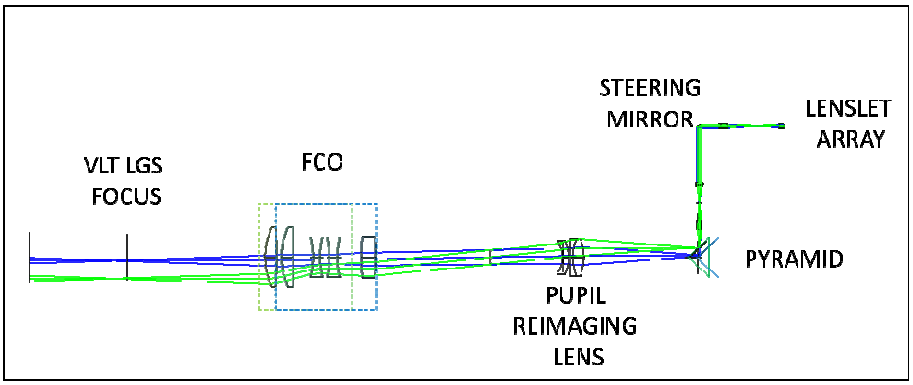

Figure 13: Left: optical scheme of the LGS path: in the center is visible the Focus Compensating Unit (FCO), in the two positions (left position: WFM, right position: NFM). A pupil is reimaged between the FCO and the first pupil reimaging lens. The pyramid on the right is shifted by 14.5mm to change from WFM to NFM (left position: WFM, right position: NFM), in order to have the light beam going to the detector always on the same path. A pupil is imaged on the jitter steering mirror, and another pupil on the detector lenslet array.

Another internal loop controls the low frequency fluctuations of the focus measured by the LGS-WFS detector: when the telescope altitude changes, the FCO will follow the Na distance according to a tracking formula tuned for the baseline zenith distance of the Na layer of 90km. The LGS-WFS will then measure a focus variation, that will be partly produced by the atmospheric turbulence (and this will be corrected by the DSM) and partly by the low frequency fluctuation of the Na layer altitude: this low frequency part of the focus variation has not to be corrected by the DSM, since, not being produced by air turbulence, does not affect the light of the observed objects. To correct the Na layer altitude variation, the low frequency fluctuations of the LGS-WFS measured focus is off-loaded to the FCO as a correction on top of the tracking movement.

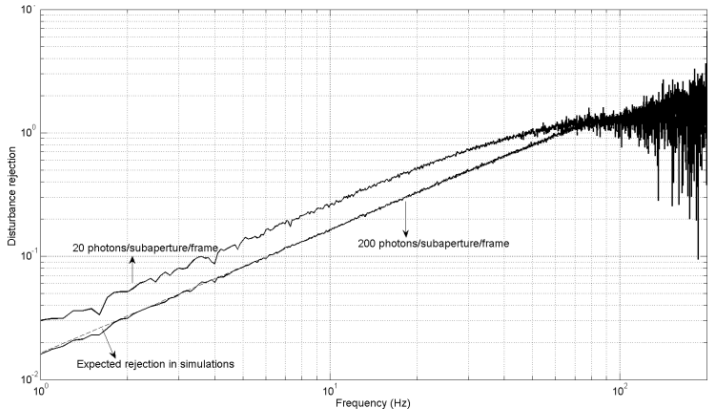

Figure 14: Right: Sensitivity function (noise rejection) of the LGS jitter loop: the two curves are in two light intensity regimes. The bandwidth is about 70 Hz, more than sufficient to control low frequency drifts, and the noise rejection at 1 Hz exceeds a factor 70. Residual tip tilt values are less than1" on sky.

This functionality has been tested and verified with the CU in GALACSI. A first quick (few sec) bootstrap correction takes care of the largest part of the defocus, due to the initial deviation of the Na layer height with respect to the expected 90km zenith altitude when the LGS is first acquired, using a slope matrix extracted by only a reduced set of SH subapertures. This speeds significantly the computation time. After this first phase, a 30s integration time feedback compensates for further low frequency focus fluctuations. This correction is performed with more accuracy using all the SH subapertures: the reduced computation speed can be accepted, since the smaller focus to be corrected requires smaller movements of the FCO. The entire focus acquisition takes about 1 minute.

3.4 Commissioning Path

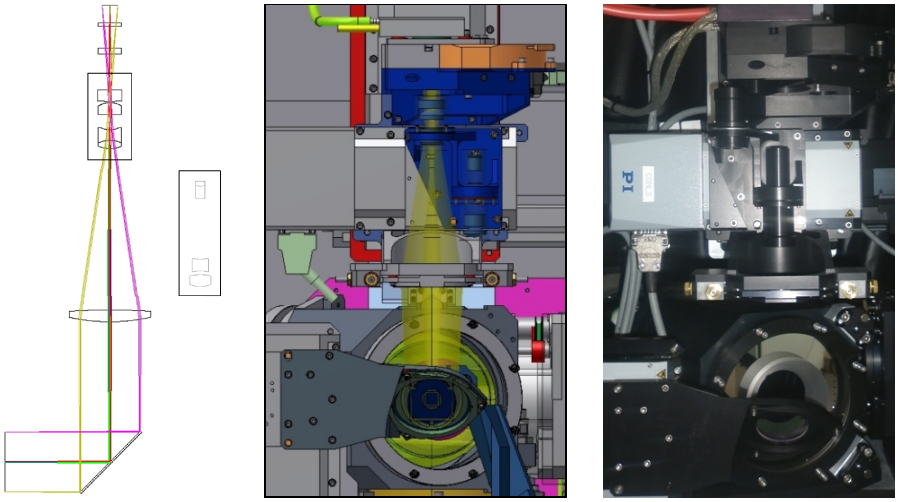

Figure 15: From left to right: optical schemes of the Commissioning path in Low Resolution (the High Resolution objective is on the right); opto-mechanical model; photo of the integrated Commissioning Path. The objective between the BS and the camera is changed to modify the scale on the camera by shifting it with a lateral translator.

In order check the MUSE field, the Commissioning Camera needs to cover the full MUSE field of 1'×1' (Low Resolution mode, LR), and to sample the diffraction limited PSF of the VLT at 650nm (High Resolution mode, HR). The system includes therefore the possibility to change the plate scale. This change is performed by moving laterally, with a translation stage, two different objectives, placed between a first relay lens and the camera (Figure 15).

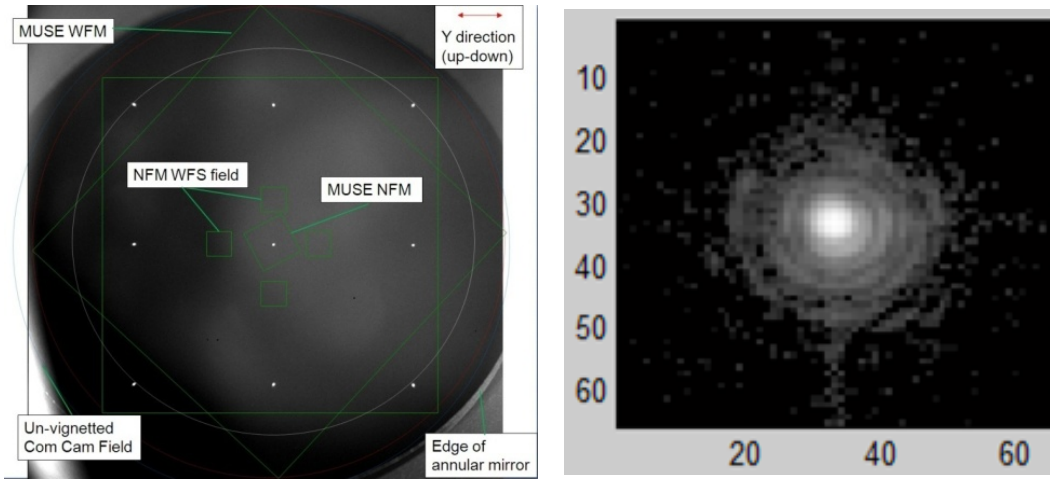

Figure 16: Left: Image of the Commissioning Camera Large Field setting. The vignetting at the corners is due to the Field splitter (annular mirror). The spots are 9 fiber sources of a temporarily installed source module with a spacing of 25.2 arc-seconds. The central one marks the Field center as defined by the Alignment tools. The MUSE and WFS field locations and centers are indicated by green squares. Right: Image of the PSF produced by the Calibration Unit on the Commissioning Camera at 852 nm, as a result of 5 exposures after dark subtraction. The Airy rings are clearly visible. The corresponding SR at this wavelength is around 75%.

In Figure 16 the Commissioning Camera field of view compared to the MUSE one is shown. The camera is mounted to the main assembly of GALCSI and co-rotating to the pupil, with the consequence that it suffers field rotation. To avoid image degradation due to the field rotation the maximum exposure time on the largest part of the sky is limited to 5s-10s.

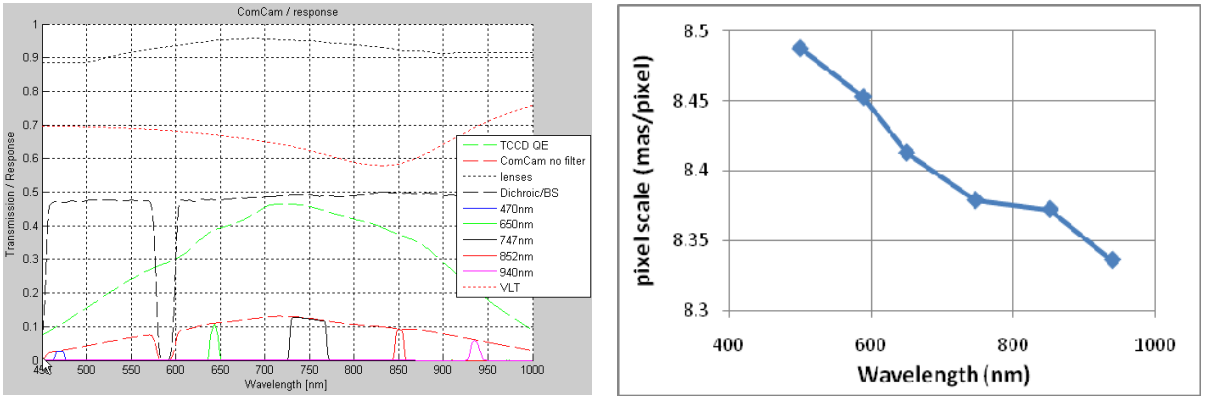

Figure 17: Left: Transmission of the Commissioning Camera without and with the narrow band filters. Right: Pixel scale in the High Resolution mode, in the whole Commissioning Camera measurement wavelength range.

Since the specifications for WFM and NFM are given at different wavelengths, a set of narrowband filters is inserted in front of the camera by a filter wheel: besides the filters at the specified wavelengths of 650nm and 747nm, a filter at 589nm to improve LGS visibility is present, plus additional 470, 852 and 940nm for NFM commissioning. The overall transmission up to the camera is shown in Figure 17.
The camera is based on a ESO Technical CCD camera using a E2V CCD 47-20 chip with 1024 by 1024 pixels. The two design pixel scales are 0.082“/pixel for the large field (LR) objective and 0.008”/pixel for the small field (HR) lens. The pixel scale has been verified for both LR and HR modes. In particular, the most critical mode, the HR reproduces well the expectations, yielding a pixel scale between 0.0083 and 0.0085”/pixel in the whole wavelength range.
The SR measurement with the diffraction limited source of the CU in HR yields values ranging from about 55 to 75 between 500nm and 940nm, with maximum between 65 and 75 between 650nm and 852nm. Taking into account that the goal is to be able to measure a SR of less than 10% at 650nm, these values meet the requirements for on-sky performance verification.

3.5 IRLOS

At the time we are writing this paper, IRLOS is still in its integration phase. The specifications and functionalities of IRLOS are described in [3]. All the internal components of the system have been however tested in standalone.

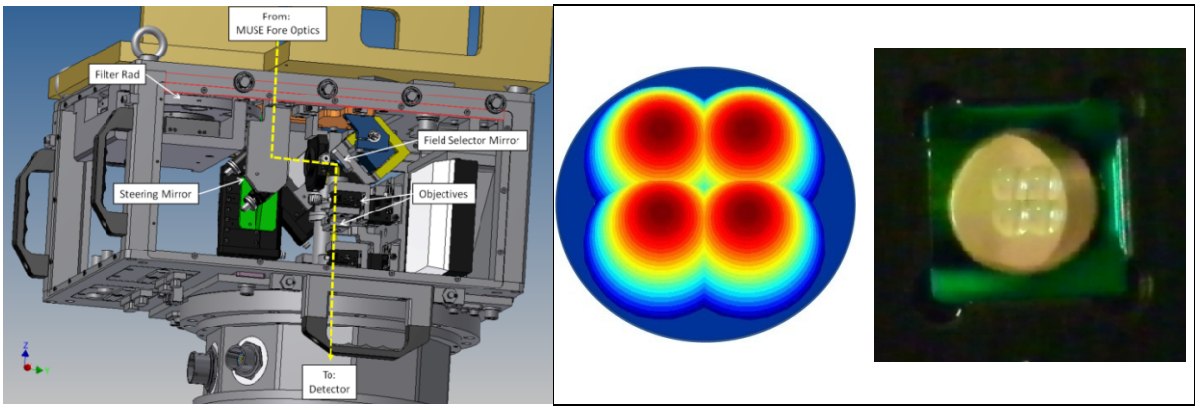

Figure 18: Left: 3D model of the IRLOS opto-mechanics: the NIR light comes MUSE Fore Optics, goes through a variable set of filter mounted on a filter rad, is deflected by a Field Selector mirror, where an internal pupil of 4.7mm diameter is imaged, passes through collimating collimation optics and reaches the detector inside a cryostat. The switch between the two plate scales (0.25" and 0.06") is obtained by shifting laterally inside the optical path the objectives with a translation stage. Each objective has its own lenslet array. Center and right: design (left) and photo of one of the two IRLOS lenslet arrays. The dimensions of the pupil is 5mm (0.06" scale, focal length=38.5mm) and 3mm (0.25" scale, focal length 5.5mm). The lenslet array is monolitic, obtained by fused silica etching.

The IRLOS assembly includes a filter wheel, a plate scale changer carrying 2 different optical barrels for the two pixel scales: 0.06"/pixel for point sources and 0.25"/pixel for extended sources. The IRLOS FS has a range of 10" on-sky. The required accuracy and repeatability of 0.005" have been extensively demonstrated. The detector, a HAWAI-I with 1024×1024 pixels and a 4 quadrant architecture, and 4 subapertures array, is hosted in an ESO continuous flow cryostat cooled to -190°C and is controlled by an ESO IR NGC controller. The 4 subapertures of the lenslet array are arranged such that one SH image falls in each quadrant: in closed loop operation only 4 small windows around the SH spots will read. 4 windows with 8×8 pixels each can be read at a frequency up to 500Hz, and a window of 20×20 pixels, that can be read at 200Hz. The detector performances have been demonstrated in standalone: background noise is lower than 900 e^-/sec ; readout noise σ_e<11 e^- RMS; acquisition at the specified frequencies of 200Hz (20×20 pixel windows) and up to 500Hz (8×8 pixel windows) is demonstrated. Two different lenslet arrays provides the spots in the two plate scale. Their design is unusual: four lenslet are realized by etching a 2mm thick plate of fused silica. Owing to the small distances of the spots, the lenslet curved faces are partially merging together. In Figure 18 (center and right) one of the two lenslet arrays (0.06" scale) is shown.

4. CONCLUSION

The integration and alignment of GALACSI in Europe is almost complete. The largest part of the specifications have been verified and most of the standalone functionalities have been, or are close to be, demonstrated. The last tests will be completed before summer 2014, with the exception of IRLOS, that will be completed around end 2014. Integration of GALACSI on the ASSIST test bench is planned for begin 2015, after the removal of GRAAL, that is currently being tested on ASSIST. Tests with the DSM will start soon after, and will last for more than six months. Shipping of GALACSI to Paranal is planned for the end of 2015.

REFERENCES

[1] Arsenault, R. et al., "ESO Adaptive Optics Facility report", Proc. SPIE Vol. 8447 844740J-1 (2012).
[2] Loupias, M.et al., "MUSE instrument global performance test", Proc. SPIE Vol.8447 84465V (2012).
[3] Stroebele, S.et al, "GALACSI System Design and Analysis", Proc. SPIE Vol. 8447 844737-1 (2012).
[4] Le Louarn, M. et al., "Wide-field adaptive optics for deep-field spectroscopy in the visible", Mon. Not. R. Astron. Soc. 349, 1009-1018 (2004).

[5] Biasi, R. et al., “VLT Deformable Secondary Mirror: integration and electromechanical tests results”, Proc. SPIE, 8447 84472G-1.
[6] Reyes, J. et al., “An overview of the ESO adaptive optics wavefront sensing camera”, Proc. SPIE, 8447, 237 (2012).
[7] Hammersley, P. et al., “The VIMOS upgrade programme”, Proc. SPIE 09/2012, DOI:10.1117/12.925132 (2012).
[8] Fedrigo, E. et al., “SPARTA: the ESO standard platform for adaptive optics real time applications”, Proc. SPIE, 6272-10 (2006).
[9] Hackenberg, W. et al., "The Four-Laser Guide Star Facility (4LGSF) for the ESO VLT Adaptive Optics Facility (AOF)", Proc. AO4ELT2 Conference (2012).
[10] Stuik, R., La Penna, P., Dupuy, C., et al. “Deploying the testbed for the VLT adaptive optics facility: ASSIST”, Proc. SPIE 8447, 118 (2012).
[11] Moussaoui, N. et al., “Statistic of the sodium layer parameters at low geographic latitude and its impact on adaptive-optics sodium laser guide star characteristics”, Astronomy and Astrophisics, 511, A31 (2010).